The exciton coupling theory of the Kasha model helps explaining the changes in the optical spectra of sulfur-bridged BODIPY DYEmers with small subchromophore distances (see figure). The preciseness of the prediction depends on the degree of electronic communication and can be estimated from a combination of optical and electrochemical analyses with DFT calculations.

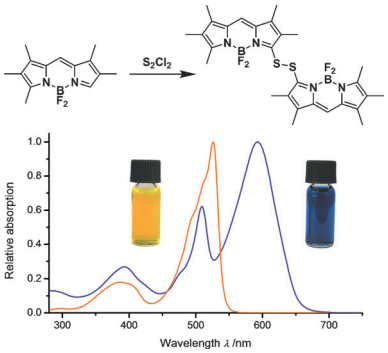

Dyes/Pigments

*J. Ahrens, B. Böker, K. Brandhorst, M. Funk, M. Bröring** ..... ▮▮▮▮–▮▮▮▮

Sulfur-Bridged BODIPY DYEmers

CHEMISTRY
A EUROPEAN JOURNAL

ChemPubSoc
Europe

DOI: 10.1002/chem.201300893

Sulfur-Bridged BODIPY DYEmers

Johannes Ahrens, Birte Böker, Kai Brandhorst, Markus Funk, and Martin Bröring*[a]

Dedicated to Professor Werner Uhl on the occasion of his 60th birthday

Abstract: Reactions of BODIPY monomers with sulfur nucleophiles and electrophiles result in the formation of new BODIPY dimers. Mono- and disulfur bridges are established, and the new dyestuff molecules were studied with respect to their structural, optical, and electrochemical properties. X-ray diffraction analyses reveal individual angulated orientations of the BODIPY subunits in all cases. DFT calculations provide solution conformers of the DYEmers which deviate in a specific manner from the crystallographic results. Clear exciton-like splittings are observed in the absorption spectra, with maxima at up to 628 nm, in combination with the expected weak fluorescence in polar solvents. A strong communication between the BODIPY subunits was detected by cyclic voltammetry, where two separated one-electron oxidation and reduction waves with peak-to-peak potential differences of 120–400 mV are observed. The qualitative applicability of the exciton model by Kasha for the interpretation of the absorption spectral shape with respect to the conformational state, subunit orientation and distance, and conjugation through the different sulfur bridges, is discussed in detail for the new BODIPY derivatives. This work is part of our concept of DYEmers, where the covalent oligomerisation of BODIPY-type dye molecules with close distances is leading to new functional dyes with predictable properties.

Keywords: BODIPY dyes · boron · DYEmers · exciton coupling · tetrapyrroles

Introduction

The boron dipyrrin complex (BODIPY, 4,4-difluoro-4-bora-3a,4a-diaza-*s*-indacene) was first described by Treibs and Kreuzer in 1968.[1] Since the late 1990s this fluorescent dye has become a topic of growing research, as the unique and positive properties of BODIPYs show prospect for much potential in manifold applications.[2] The high chemical and physical stability, as well as well-defined absorption and fluorescence spectra with high quantum yields, are representative features of BODIPYs.[3] Many different architectures and derivatizations on the BODIPY core are aiming at the alteration of photophysical properties and/or the implementation of functionality, and have successfully been applied to this class of dyes. Large red-shifts into the NIR region,[4] large Stokes shifts in combination with high fluorescence quantum yields,[5] and water solubility[6] have been some of the key points in this erupting field of research. Furthermore, specific connectivities can be chosen synthetically to take advantage of the potential of this luminescent dye for many diverse optoelectronic applications.[7]

One current aspect of the development of BODIPY chemistry is the integration of the chromophore into polymers and oligomers.[8,9] Depending on the position (α (3,5), β (2,6), β′ (1,7), *meso* (8), and boron (4); see Figure 1) and the linkage (distance, orientation, electronic coupling), more or less interaction can be observed between the BODIPY subunits by photophysical and/or electrochemical methods.[8] Especially for dimers with close interchromophoric distances significant property changes can be expected and have recently been studied for the first examples.[10–12] Nevertheless, the number of reports on well-defined BODIPY oligomers is still limited.[13,14] Due to the well-developed synthetic addressability of the BODIPY framework, we have coined the term "DYEmers" for this class of BODIPY oligomers with systematically altered bridging patterns. Recently, we have introduced BODIPY DYEmers with one direct C–C connection and reported about their new properties like exceptional large Stokes shift with high fluorescence quantum yield.[11,15]

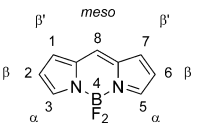

Figure 1. BODIPY core structure with numbering scheme and nomenclature.

An intriguing possibility for bridging two BODIPY chromophores at different positions is given by the use of sulfur-based connecting units. Due to the possibility of an electronic conjugation of the subchromophores through the sulfur atom(s) it is in question, whether the absorption spectra of

[a] J. Ahrens, B. Böker, Dr. K. Brandhorst, Dr. M. Funk, Prof. Dr. M. Bröring
Institut für Anorganische und Analytische Chemie
Technische Universität Braunschweig
Hagenring 30, 38106 Braunschweig (Germany)
Fax: (+49) 531-391-5387
E-mail: m.broering@tu-bs.de

Supporting information for this article is available on the WWW under http://dx.doi.org/10.1002/chem.201300893: Synthetic procedures for **2**, **3**, and **4**; ^{1}H, ^{13}C, ^{19}F, ^{11}B NMR spectra of all compounds; cyclic voltammograms of **8** and **11**.

such DYEmers could still be described, or even predicted, by the simple exciton coupling model of Kasha.[16] In this contribution we present preparative routes towards different dimers derivatives, describe their solid state and solution structures as well as their photophysical and electrochemical characterization, and discuss the applicability of Kasha's model to each of the sulfur-bridged BODIPY DYEmers.

Results and Discussion

Synthesis: Two different synthetic strategies have been tested in order to obtain sulfur-brigded symmetrical dimers of BODIPYs linked at the α-positions, a nucleophilic one[17,18] using sulfide anions as the sulfur source in S_NAr reactions, and an electrophilic one employing sulfur chlorides.[19,20] Therefore, the α-free BODIPY **3** and the 3-bromo BODIPY **4** were chosen as unsymmetrical BODIPYs with one reactive position (Scheme 1; for details see Supporting Information). Note that the free *meso*-position of BODIPYs is reactive only towards very strong nucleophiles such as *n*BuLi.[21] Compounds **3** and **4** were obtained by BF_2 complexation of the corresponding dipyrrin hydrobromides **1**[22] and **2**. Compound **2** was prepared from **1** by treatment with elemental bromine.[23]

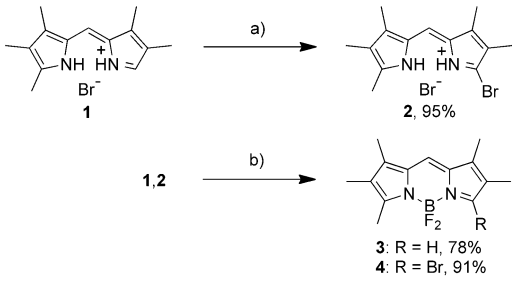

Scheme 1. Syntheses of BODIPY starting materials **3** and **4**: a) 1) Br_2, CH_2Cl_2, RT, 30 min, 2) cyclohexene, Et_2O; b) 1) NEt_3, CH_2Cl_2, 2) $BF_3{\cdot}OEt_2$, RT, 1 h.

The unsymmetrical 3-bromo BODIPY **4** was successfully dimerized to the desired thioether **5** in 56% yield by treatment with sodium sulfide as the nucleophile in toluene/water at reflux and under phase-transfer conditions (Scheme 2). Similarly, the symmetrical disulfide **6** forms from **4** in 67% yield using a freshly prepared solution of

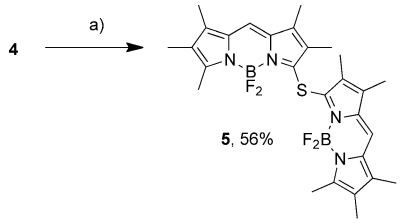

Scheme 2. Nucleophilic substitution to dimeric BODIPY sulfide **5**: a) $Na_2S{\cdot}9H_2O$, nBu_4NBr, toluene, reflux, 3.5 h.

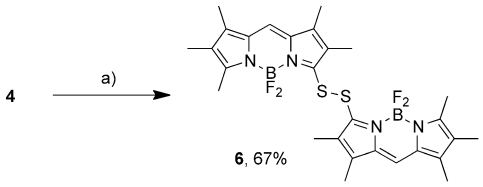

Scheme 3. Nucleophilic substitution to dimeric BODIPY disulfide **6**: a) Na_2S_2, MeOH, CH_2Cl_2, RT, 25 min.

sodium disulfide in MeOH. This latter reaction, however, requires much less forcing conditions (CH_2Cl_2, RT) due to the more pronounced nucleophilicity of the disulfide (Scheme 3).

During the search for suitable reaction conditions towards the disulfide **6**, the formation of the dipyrrin-1-thione **7** from **4**, sodium sulfide, and elemental sulfur was observed (Scheme 4). Surprisingly, the rather tightly bound BF_2 unit of **4** is lost in the process of bromine substitution. To the best of our knowledge, a similar result has only once be reported for a 3-amino BODIPY, which also loses the BF_2 group upon addition of acid.[24] Analytical and spectroscopic data of **7** are in good agreement with those known from a dipyrrin-1-thione study performed by Lightner.[25] In this case, however, the sulfur atom has been introduced by the action of Lawesson's reagent onto the corresponding dipyrrinone. For comparison, the unsymmetrical BODIPY thioether **8** has been produced by nucleophilic substitution of **4** with 4-tolylthiol (Scheme 4).

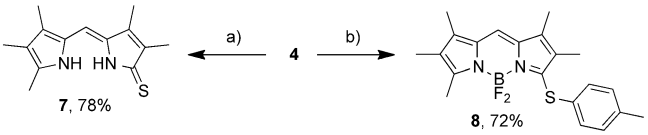

Scheme 4. Deboronation reaction to **7** and nucleophilic substitution to **8**: a) $Na_2S{\cdot}9H_2O$, S_8, EtOH, toluene, 90 °C; b) 4-methylthiophenole, NEt_3, MeCN, CH_2Cl_2, RT, 15 min.

A second general preparative entry towards the DYEmers **5** and **6** is the use of electrophilic sulfur halides in terms of a S_EAr reaction. Following this approach the α-unsubstituted pentamethyl BODIPY **3** reacts with sulfur dichloride (SCl_2) in dichloromethane to yield sulfide **5** in a diminished yield of 24% (Scheme 5). If sulfur monochloride (S_2Cl_2) is used instead, **3** is transformed into a mixture of symmetrical BODIPY dimers bridged by polysulfides of different lengths. Only the sulfide **5** and the disulfide **6** could be isolated after column chromatography in yields of 21 and 33%, respectively (Scheme 5). The trisulfide and higher polysulfides were detected by ESI mass spectrometry, but seem to interconvert with time, yielding mainly **5** and **6**. The occurrence of sulfur bridges of different length in the substitution products of S_2Cl_2 and their thermodynamic conversion has been reported earlier for related oligopyrrolic macrocycles.[20]

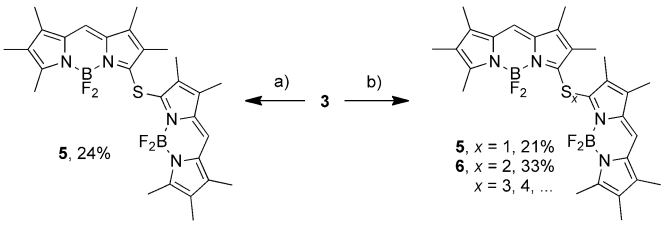

Scheme 5. Electrophilic substitution of **3** and formation of DYEmers **5** and **6**: a) SCl_2, CH_2Cl_2, 0 °C → RT; b) S_2Cl_2, CH_2Cl_2, −65 °C → RT.

For the introduction of a sulfur bridge at the β-position (2,6-position) only the electrophilic route is feasible, as for the nucleophilic route an electron poor (vinylogous) iminium halide function (3,5- and 1,7- and 8-positions) is required.[17,26–28] The known pentaalkylated BODIPY **9**[29] was reacted with sulfur monochloride in dichloromethane at low temperature (Scheme 6). Interestingly, only the sulfide **10** could be isolated after column chromatography in low yield as the main product, while a disulfide species could only be detected in a different fraction by ESI mass spectrometry.

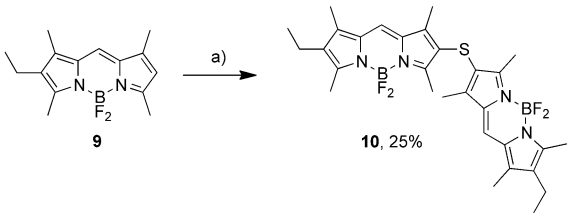

Scheme 6. Electrophilic substitution to DYEmer **10**: a) S_2Cl_2, CH_2Cl_2, −70 °C, 2 h.

As for the α-substituted examples, a monomeric β-tolylthio derivative **11** was prepared for comparison. Therefore, the necessary 4-tolylsulfenyl chloride was prepared in situ from *N*-chlorosuccinimide and 4-tolylthiol,[30] and reacted with **9** to result in the desired thioether **11** in 96% yield (Scheme 7).

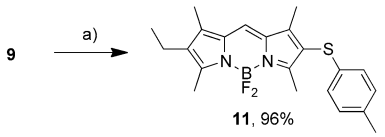

Scheme 7. Electrophilic substitution to thioether **11**: a) 1) 4-Tolylthiol, NCS, RT, 30 min; 2) **9**, 0 °C, 15 min.

In solution, the dimeric dyes **5**, **6**, and **10** are clearly distinct from the monomers **3**, **4**, **8**, **9** and **11** in several aspects. Most obvious is the color change from orange-yellow with intense yellowish-green fluorescence for solutions of the monomeric starting materials (**3**, **4**, and **9**) to blue and blue-violet, respectively, without visible fluorescence by naked eye for CH_2Cl_2 solutions of the dimers **5** and **6**. This change is less pronounced, though still apparent for the dimer **10** which shows a violet-red color and no visible fluorescence in CH_2Cl_2 solution.

Solid state X-ray structures of 5, 6, 8, 10, and 11: The three new sulfur-bridged DYEmers **5**, **6**, and **10** as well as the thioether monomers **8** and **11** were studied by single-crystal X-ray diffraction (Figure 2–6). The sulfide **5** crystallizes in the space group $P\bar{1}$ with one dye molecule in the asymmetric unit. For the disulfide **6** the same triclinic space group is found with $Z=2$. However, one molecule of co-crystallized solvent is found per formula unit. This solvent is severely disordered and has been removed from the electron density map using the SQUEEZE command in PLATON.[31] The BODIPY subunit structures of **5** and **6** deviate very slightly from each other. However, each of the BODIPY units is characterized by a nearly flat C_9BN_2 framework, and by angles at the boron atom close to 109.5°. These structural characteristics do not deviate significantly from those of monomeric BODIPYs such as **8**. The sulfur bridge in **5** is described by bond lengths C9–S1 of 1.755(2) Å and C10–S1 of 1.752(2) Å and a bond angle C9-S1-C10 of 100.5(1)°, which are very similar to the values from a crystal structure of 10-thiabilirubin[32] and similar to **8** (C14–S1 1.762(4) Å, C14-S1-C15 103.3(2)°). The disulfur bridge in **6** shows bond lengths C9–S1 of 1.749(2) Å, C10–S2 of 1.744(2) Å, and S1–S2 of 2.088(1) Å, bond angles C9-S1-S2 and C10-S2-S1 of 103.0(1) and 102.6(1)°, respectively, and a dihedral angle C9-S1-S2-C10 of 94.5(1)°. These values are similar to those of a bis(bipyrroledisulfide) macrocycle.[20] The β-bridged sulfide **10** crystallizes in the orthorhombic space group *Pnc*2 with two dye molecules in the asymmetric unit. The molecular geometries of the independent molecules of **10** differ slightly, but insignificantly from each other, and show very similar characteristics as the monomeric **11**. For discussion, one molecule was chosen. The BODIPY subunit structures of **10** show crystallographic symmetry and are connected by a sulfur atom with bond lengths C2/C2a–S1 of 1.756(3) Å and a bond angle C2-S1-C2a of 103.6(1)°. Table 1 summarizes selected molecular data for the new derivatives.

The intramolecular arrangement of the monomeric subunits is of special interest for the photophysical behavior of **5**, **6**, and **10**. For the case of **5**, this arrangement is described by a dihedral angle ϕ of 71.0(1)° between the C_9BN_2 mean planes, a distance of 7.803(1) Å between the centers of the BODIPY moieties R, and by the closest distance between fluorine atoms of different BF_2 groups d_{FF} of F2···F4 of 5.447(2) Å (Figure 2). Apparently, the orientation of the subchromophores of **6** deviates significantly, and the BODIPY units are also further apart from each other (Figure 3). This is quantified by a dihedral angle of ϕ = 33.2(1)° between the C_9BN_2 mean planes, an intercenter distance R of the BODIPY moieties of 8.541(1) Å, and the closest distance between fluorine atoms of different BF_2 groups (F2···F3) of $d_{FF}=5.729(2)$ Å. The angulated structure of **10** finally leads to values for the dihedral angle of $\phi=$ 79.7(1)°, for the distance between BODIPY centers of $R=$

Table 1. Selected bond lengths [Å], distances [Å], and bond angles [°] for **5**, **6**, **8**, **10**, and **11**.

	5	6	8	10[a]	11
B1–N1	1.555(3)	1.567(3)	1.536(5)	1.554(4)	1.552(2)
B1–N2	1.546(2)	1.556(3)	1.557(5)	1.549(4)	1.551(2)
B2–N3	1.561(2)	1.550(3)	–	[b]	–
B2–N4	1.558(2)	1.568(3)	–	[b]	–
B1–F1	1.393(2)	1.392(3)	1.380(5)	1.386(4)	1.391(2)
B1–F2	1.394(2)	1.380(3)	1.386(5)	1.396(3)	1.391(2)
B2–F3	1.385(2)	1.382(3)	–	[b]	–
B2–F4	1.394(2)	1.388(3)	–	[b]	–
N1···N2	2.491(2)	2.493(2)	2.484(4)	2.488(3)	2.489(2)
N3···N4	2.504(2)	2.495(2)	–	[b]	–
N1-B1-N2	106.9(1)	106.0(2)	106.9(3)	106.6(2)	106.7(1)
N3-B2-N4	106.8(1)	106.3(2)	–	[b]	–
F1-B1-F2	109.7(1)	109.8(2)	109.8(3)	109.1(2)	109.0(1)
F3-B2-F4	109.0(1)	110.3(2)	–	[b]	–

[a] Data given only for one of the two crystallographically independent molecules. [b] Due to a symmetry operation (two-fold rotational axis) the halves of a molecule of **10** are crystallographically identical.

8.193(1) Å, and for the closest distance between fluorine atoms (F1···F1a) of $d_{FF}=7.518(2)$ Å (Figure 5).

The intermolecular contacts between the BODIPY units of the DYEmers are mainly based on π-stacking interactions. For **5**, **6**, and **10**, however, different types of arrangements are evident from the crystal structures. The α-connected sulfide **5** shows pairs of antiparallel stacked BODIPY moieties in distances of 3.448 and 3.561 Å. Both BODIPY subunits of a given molecule show short contacts to different neighbors and form supramolecular 1D polymeric strands. The interaction of the second side of each BODIPY is inhibited sterically by a methyl group of the respective other half of the molecule (at C8 and C11, see Figure 2). Compound **6** forms two distinct and loosely stacked columns in the crystal. These columns contain BODIPY subunits in distances between 3.461 and 3.813 Å and progress in two orientations along the crystallographic *a* direction. **10** finally contains tilted and slipped stacks in estimated distances of 3.39 and 3.70 Å. These stacks are pointing in two different directions, which organizes the DYEmer molecules in a zig-zag orientation towards each other.

DFT structures and solution dynamics: For an analysis of the influence of the different π-stacking interactions of the sulfur-bridged DYEmers on the conformation and intrachro-

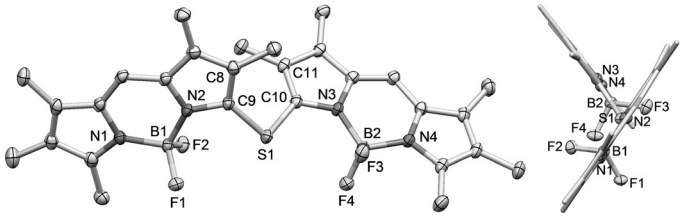

Figure 2. Molecular structure of **5** (ellipsoids set at 50% probability; hydrogen atoms omitted for clarity). Left: View of the complete molecule. Right: View along the intersection line of the C_9BN_2 mean squares planes.

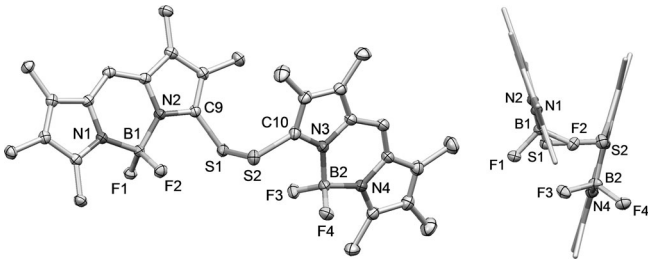

Figure 3. Molecular structure of **6** (ellipsoids set at 50% probability; hydrogen atoms omitted for clarity). Left: View of the complete molecule. Right: View along the intersection line of the C_9BN_2 mean squares planes.

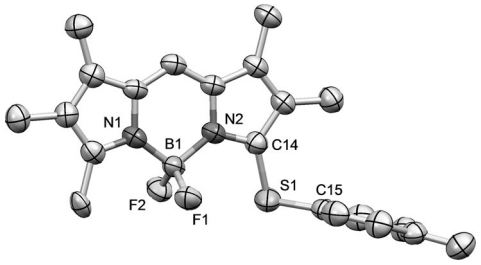

Figure 4. Molecular structure of **8** (ellipsoids set at 50% probability; hydrogen atoms omitted for clarity).

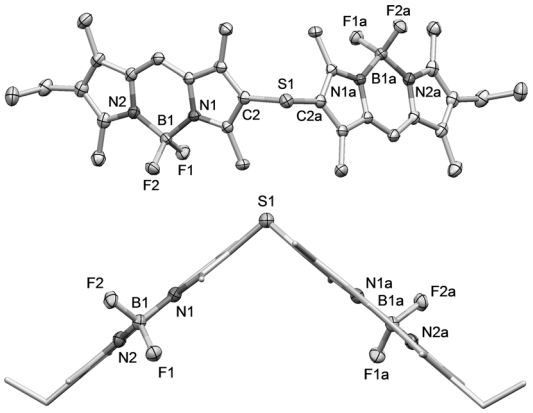

Figure 5. Molecular structure of **10** (ellipsoids set at 50% probability; hydrogen atoms omitted for clarity). Top: View of the complete molecule. Bottom: View along the intersection line of the C_9BN_2 mean squares planes.

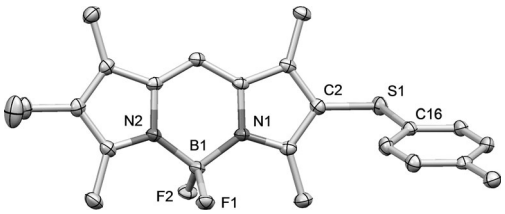

Figure 6. Molecular structure of **11** (ellipsoids set at 50% probability; hydrogen atoms omitted for clarity).

mophore arrangement, DFT calculations of the solution structures of **5**, **6**, and **10′**[33] have been undertaken. A conformational analysis using the OPLS_2005 force field and a Monte Carlo sampling was first carried out to find low-energy conformations of the compounds in dichloromethane solution, which were then further optimized using density functional theory (B3LYP/6-31G(d,p)). The results of these calculations are given in Figures 7–9.

For **5**, a stretched main conformer **5-I** is found in solution, for which a weak electronic conjugation of the BODIPY units appears feasible via a free 3p orbital of the bridging sulfur atom. The energetically closest conformer **5-II** is found 17.46 kJ mol^{-1} above the stretched form (Figure 7). This high-energy conformer is characterized by a compact overall structure with a small distance between the BODIPY unit centers R of 3.668 Å, and an increased dihedral angle ϕ between the BODIPY planes of 83.19°. As the population of this conformer should be low, a rigid and stretched out structure may be proposed for **5** in solution (compare ^{19}F NMR study below). Disulfide **6** resides in solution in three geometrically quite different conformers **6-I**–**6-III** (Figure 8) which are energetically very similar, so that a high conformational flexibility should result. The β-bridged sulfide **10′** also shows three energetically and structurally similar conformers **10′-I**–**10′-III** (Figure 9). These conformers are distinct by different relative rotational states of the BODIPY moieties, and therefore by the relative orientation of the permanent dipol moments of the monomeric subunits. Obviously, these permanent dipoles play only a minor role for the stabilization of a certain conformer. Generally, it is obvious that the energetical minimum conformations from the solution calculations **5-I**, **6-I**, and **10′-I** are structurally equivalent to the conformations found in the crystal lattices of the DYEmers **5**, **6**, and **10**. Structural deviations by π stacking and other packing effects are minor and mainly effective by small rotations of one (**5**, **6**) or two (**10**) of the BODIPY units along the C–S axis.

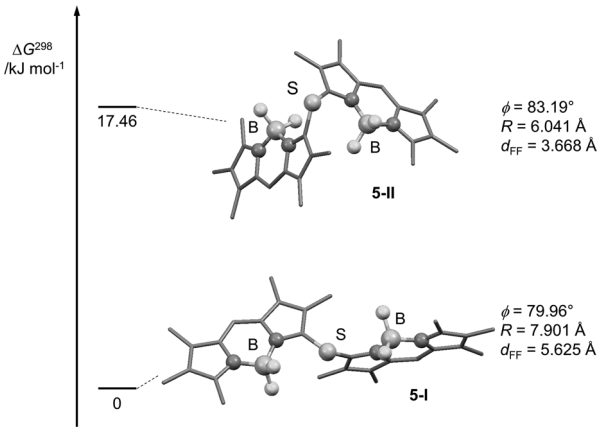

Figure 7. Calculated solution structures for the low-energy conformations of **5** (B3LYP/6-31G(d,p), CH_2Cl_2; H atoms removed for clarity), with relative energy levels and characteristic metrics (see text).

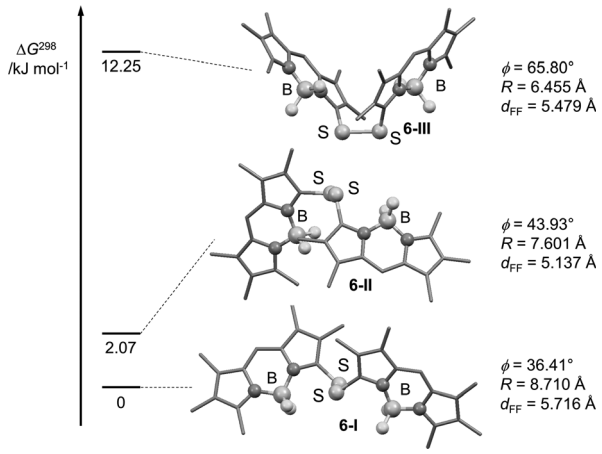

Figure 8. Calculated solution structures for the low-energy conformations of **6** (B3LYP/6-31G(d,p), CH_2Cl_2; H atoms removed for clarity), with relative energy levels and characteristic metrics (see text).

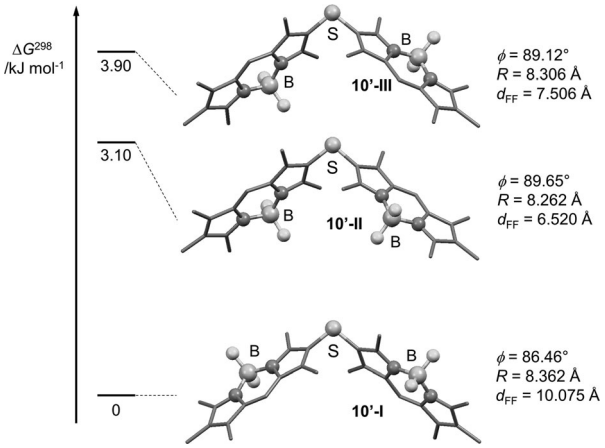

Figure 9. Calculated solution structures for the low-energy conformations of **10′** (B3LYP/6-31G(d,p), CH_2Cl_2; H atoms removed for clarity), with relative energy levels and characteristic metrics (see text).

As another aspect of the solution structures of the DYEmers **5**, **6**, and **10**, the NMR characterisation of the three new BODIPY dimers reveals a special feature. In the ^{19}F NMR spectrum of **5**, two broad and unspecific signals at $\delta \approx -139$ and -148 ppm appear at ambient temperature. These signals indicate two different fluorine positions and dynamic behavior for the symmetric compound. In contrast, the disulfide **6** and the sulfide **10** give a single quartet in the ^{19}F NMR spectrum ($\delta \approx -142$ and -147 ppm, respectively) under the same conditions, which is typical for BODIPYs with equal positions of the fluorine atoms, like for example for **8** or **11**. Apparently, for **5** the rotation of the two BODIPY units relative to each other is sterically hindered. The effect is reminiscent to the behavior of BODIPY dimers with direct C–C connections. These DYEmers possess a rigid angulated structure and were studied in detail by NMR spectroscopy at room temperature.[11,34]

For sulfide **5** the two broad ^{19}F signals are sharpening upon lowering the temperature stepwise from 300 to 213 K (Figure 10, right), and complex coupling patterns appear for both signals. This reveals that the S-bridged BODIPY dimer **5** resides in a locked conformation and behaves similar to directly coupled DYEmers. Upon heating the signals broaden, and coalescence is observed at ~344 K (Figure 10, left). The broad signal for the fast exchange is observed at a chemical shift of $\delta \approx -143$ ppm, typical for rotationally unhindered BODIPYs such as **8**. From the coalescence temperature of $T_c = 344(2)$ K and a peak separation of 3300 Hz, the free energy of activation can be estimated to $\Delta G^{\neq} = 59.2(4)$ kJ mol^{-1} for this rotational process.

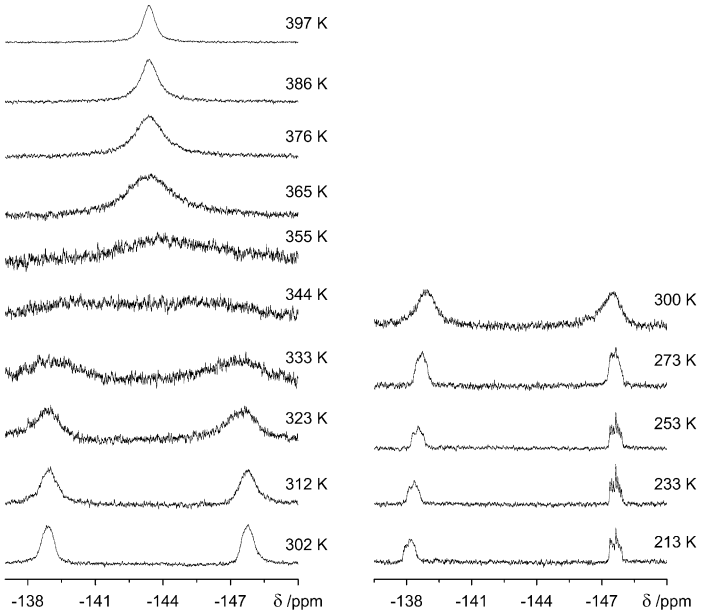

Figure 10. ^{19}F NMR spectra of **5** at different temperatures (376 Hz; left side: high temperatures with coalescence, $C_2D_2Cl_4$; right side: low temperatures, CD_2Cl_2).

Photophysical properties: All BODIPY compounds were examined by absorption and steady-state fluorescence spectroscopy in dichloromethane, and the results are summarized in Table 2. Thioether **8** shows typical optical spectra for a simple monomeric BODIPY (Figure 11). The shape of the absorption spectrum is described by one main band at 545.0 nm, which is assigned to a strong $S_1 \leftarrow S_0$ transition, and one weaker, broad band at 384.0 nm attributed to the $S_2 \leftarrow S_0$ transition.[3] The excitation spectrum registered on the emission maximum is similar to the absorption spectrum. The intense fluorescence of **8** occurs from the $S_1 \rightarrow S_0$ transition in a mirror-shape band with a Stokes shift of 27 nm at 572 nm ($\Phi_f = 0.82$ in CH_2Cl_2). The spectra of **8** are bathochromically shifted relative to the α-free BODIPY **3** due to the electron-rich sulfur substituent.[35] The red-shift for the main absorption of the monomeric reference **11** relative to the starting material **9** is much less pronounced (Table 2 and Figure 12). Interestingly, however, the Stokes shift of 76 nm is much larger for the β-substituted BODIPY than for **8**, and accompanied by a smaller quantum yield of 0.27 in CH_2Cl_2. This differing optical behavior appears to depend on the site of substitution alone and was found earlier for regioisomeric BODIPYs with one alkynyl substituent.[27,36]

Table 2. Photophysical properties of the BODIPYs in CH_2Cl_2 at room temperature.

Compound	Absorption		Fluorescence	
	λ_{max} [nm]	ε [10^4 L mol^{-1} cm^{-1}]	λ_{max} [nm]	Φ_f[a]
3	388.0	1.6	536	0.84
	526.0	8.8		
4	381.0	1.2	542	0.57
	532.0	9.1		
5	388.0	1.4	652	~0.007[b]
	510.5	2.0		
	628.5	12.2		
6	393.5	1.3	659	~0.006[b]
	509.0	4.4		
	592.0	7.1		
8	384.0	1.6	572	0.82
	545.0	9.0		
9	374.0	0.7	532	0.97
	520.0	8.0		
10	389.0	1.7	614	~0.005[b]
	507.0	4.8		
	551.0	10.5		
11	387.0	0.8	600	0.27
	524.0	6.9		

[a] Absolute fluorescence quantum yields in aerated solvent using an integrating sphere. [b] Note ref. [37].

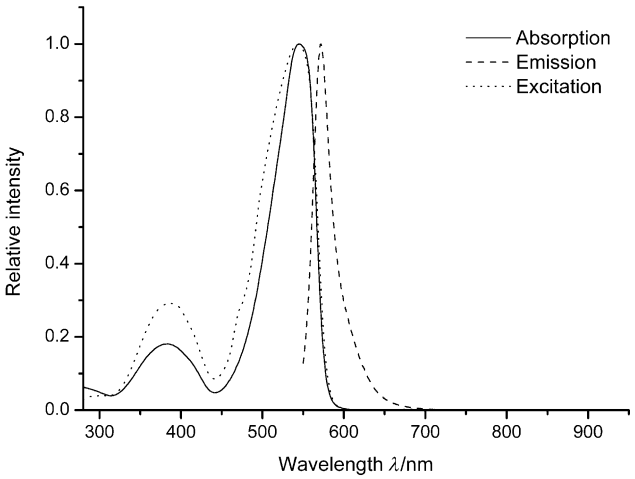

Figure 11. Optical spectra of **8** recorded in CH_2Cl_2.

In the absorption spectra of the two different dimers bridged through the α-positions the expected exciton coupling with splitting of the S_1 level is observed. This typical DYEmer behavior is likely due to the close spatial relationship of the non-conjugated (or only weakly conjugated) subchromophores, and to the observed conformational characteristics.[16] The electronic transition dipole moment for the $S_1 \leftarrow S_0$ transition of a BODIPY unit is perpendicular (i.e., along the 2,6-positions) to the C_{2v} symmetry axis of the core,

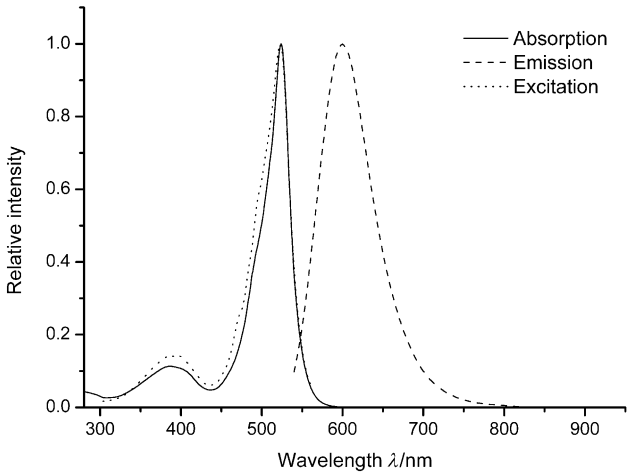

Figure 12. Optical spectra of **11** recorded in CH_2Cl_2.

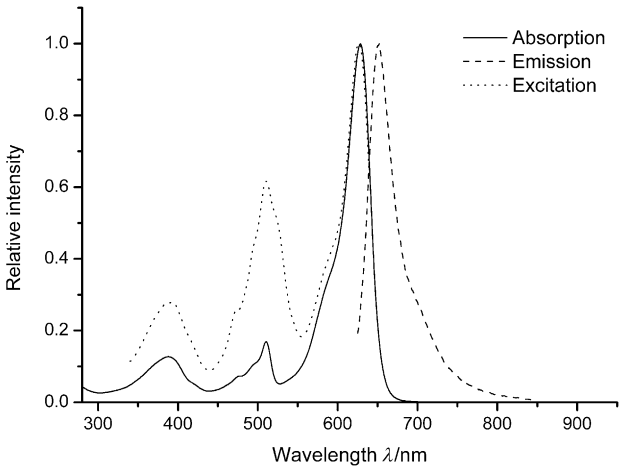

Figure 13. Optical spectra of **5** recorded in CH_2Cl_2.

which is in direction of the permanent electric dipole moment from the boron atom to the *meso*-position.[38] Thus, the absorption spectrum of the sulfide **5** in CH_2Cl_2 shows three bands (Figure 13), one weak, broad band at 388.0 nm for the $S_2 \leftarrow S_0$ transition and two bands for exciton split $S_1 \leftarrow S_0$ transitions according to the model of Kasha. One of these latter bands at 510.5 nm has a small higher-energetic shoulder and is hypsochromically shifted relative to the monomeric **8**, while the other band at 628.5 nm is far bathochromically shifted, which results in a large exciton splitting of 118 nm. The split band to lower energy is much more intense than the high-energy band, which accounts for a stretched and only moderately angular alignment of the transition dipole moments of the BODIPY subunits in solution.[16] The intramolecular nature of this phenomenon was proven by absorption spectra from a dilution series. No concentration effects on band position and molar absorption coefficient could be observed from 10^{-4} to 10^{-6} mol L^{-1} in CH_2Cl_2. The fluorescence emission of **5** occurs in one band with a small Stokes shift at ~650 nm and is quenched in polar solvents ($\Phi_f = \sim 0.007$ in CH_2Cl_2). In non-polar solvents with only poor solubility of **5** this dimer shows a visible red fluorescence, and significantly higher fluorescence quantum yields were determined ($\Phi_f = 0.44$ in *n*-hexane; $\Phi_f = 0.11$ in toluene). The excitation spectrum shows three bands at positions similar to the absorption spectrum. Variation of the solvent exhibits a dependence of the absorption and emission energies of **5** on the solvent polarity, resulting in a negative solvatochromism. For MeCN, MeOH, EtOAc, CH_2Cl_2, Et_2O, *n*-hexane, and toluene, a shift of $\lambda_{max,abs}$ from 616 to 639 nm and of $\lambda_{max,em}$ from 639 to 655 nm is observed. Such a behavior is generally typical for monomeric BODIPYs,[39] but appears to be much stronger for DYEmers.

The absorption spectrum of disulfide **6** also shows a split low-energy absorption in CH_2Cl_2 (Figure 14). In this case, however, the exciton splitting of 83 nm is smaller than for **5**. The low-energy band at 592.0 nm is less red-shifted as in the spectrum of **5** and similar to the signal of monomeric **8**. The second band at 509.0 nm is more intense than the respective band in the spectrum of **5**. This difference in relative intensities suggests a more tilted alignment of the transition dipole moments of the subchromophores of **6** in solution. Furthermore, the smaller exciton splitting can be ascribed to the increased distance of the BODIPY subunits in the disulfide compared to the sulfide.[16] The $S_2 \leftarrow S_0$ transitions in the spectra of both dimers show one broad, weak band, which implies little exciton coupling for the S_2 level. The fluorescence emission of **6** occurs at 659 nm ($\lambda_{exc} = 592$ nm) and is quenched in CH_2Cl_2 ($\Phi_f = \sim 0.006$) as well as in toluene. Quite unexpectedly, only two bands are present in the excitation spectrum, a larger one at the $S_2 \leftarrow S_0$ transition region, and a smaller one in the center of the split main absorption bands at 532 nm.

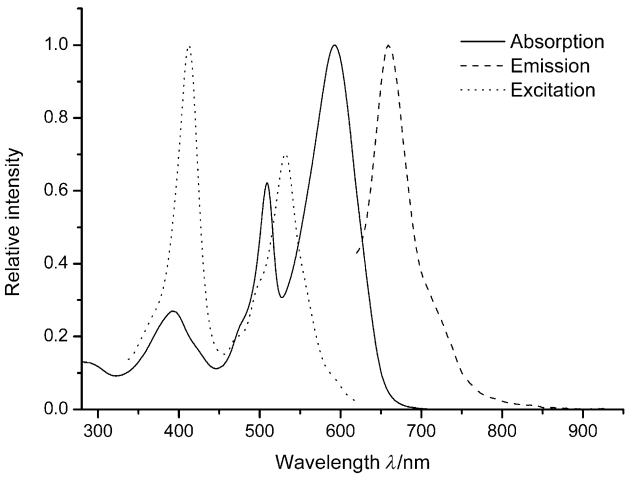

Figure 14. Optical spectra of **6** recorded in CH_2Cl_2.

The β-bridged sulfide **10** produces yet different optical spectra (Figure 15). The exciton coupling is not as pronounced as for the α-bridged DYEmers **5** and **6** and results for the $S_1 \leftarrow S_0$ transition in an intense band at 551.0 nm with a distinct shoulder at 507.0 nm. As for the other dimers, the

exciton coupling on the S_2 level of **10** is only of minor importance. The small exciton splitting of 44 nm can be explained by assuming an increased distance of the subunits in **10** compared to **5** or **6**, and the lower intensity of the high-energy band accounts for a more linear alignment of the transition dipole moments of the subchromophores of **10** in solution. The relative excitonic coupling strengths of **5** and **10** coincidence with those of the directly C–C coupled BODIPY dimers. Here, the α-coupled homodimers show a large split of the main absorption,[11,15,40] whereas for the β-coupled homodimers only a bathochromic shift is found.[14] The influence on the absorption spectra thus appears to be depending on the linking position. In the fluorescence spectrum **10** emits with a Stokes shift of 63 nm at 614 nm, and the fluorescence is largely quenched in CH_2Cl_2 ($\Phi_f = \sim 0.005$) as for **5** and **6**. In non-polar toluene, however, a much higher fluorescence quantum yield of 0.42 is observed. The excitation spectrum of **10** follows the absorption spectrum and supports, that the $S_1 \leftarrow S_0$ transition is slightly split.

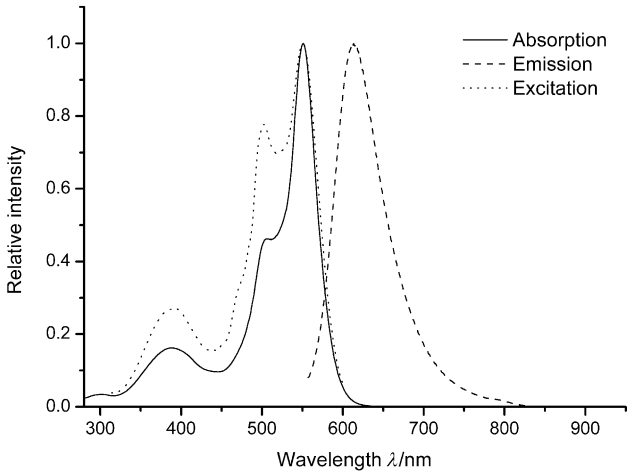

Figure 15. Optical spectra of **10** recorded in CH_2Cl_2.

For both sulfides **5** and **10**, the fluorescence quantum yield is reduced in polar dichloromethane and strongly enhanced in unpolar solvents such as toluene, while no significant changes are observed in absorption (meaning that the ground state conformation is almost independent of the solvent), despite from the negative solvatochromism. This behavior suggests an intramolecular charge transfer (ICT) process in the excited state under solvent-induced symmetry breaking. For other BODIPY DYEmers, but without a bridging heteroatom (C–C and methylene bridge), the same conclusion was drawn and discussed in more detail by Thompson[10d] and Ziessel[10f]. In the case of the disulfide **6**, the singlet quantum yield is low regardless of the solvent polarity. The unusual excitation spectrum of **6** in combination with the accessibility of several low-lying conformers may be interpreted in terms of an intramolecular excimer formation independent of the solvent. However, due to the uncertain influence of the sulfur atoms, and to a probable radiationless deactivation process through rotation along the S–S axis of **6**, these points have to remain highly speculative suggestions until detailed lifetime analyses are available.

Analyses of excitonic couplings: The model of exciton coupling[16,41–43] considers a dimer of two identical (or similar) chromophores A and B, which are connected covalently without conjugation (or are aggregated). The coupling is described as an electrostatic interaction between the transition dipole moments μ_{eg} of the two subchromophores leading to an energy splitting of the excited state. Only the strong coupling case is assumed by this model elaborated for molecular dimers by Kasha.[16] In this model, V_{AB} is the energy of the exciton splitting, also called Davydov splitting,[44] which is twice the energy of the exciton interaction. This energy can be written after a point-dipole point-dipole approximation of the transition dipole moments as Equation (1):

$$V_{AB} = 2\frac{\left(\mu_{eg}^{monomer}\right)^2}{4\pi\varepsilon_0 n^2 R^3}\kappa \qquad (1)$$

where $\mu_{eg}^{monomer}$ is the value of the transition dipole moment of the monomer, R the intradimeric distance between the centers of the transition dipole moments and κ the orientation factor. The orientation factor describes the angle relation between the subchromophoric transition dipole moments relative to the center-to-center distance vector (Figure 16) as described in Equation (2):

$$\kappa = \cos\theta_{AB} - 3\cos\theta_A \cos\theta_B \qquad (2)$$

where θ_A and θ_B are the angles between the transition dipole moment of the corresponding subchromophore and the distance vector and θ_{AB} the angle between both dipole

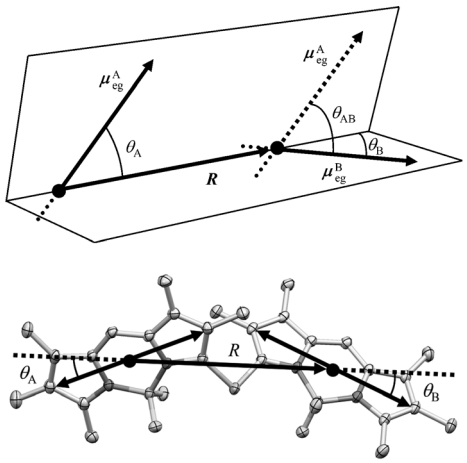

Figure 16. Top: Angular relationship between the transition dipole moments of A and B connected by the distance vector ***R*** to determine the orientation factor κ. Bottom: Example for determination of the angles θ_A, θ_B, and θ_{AB} (not shown), and of the center-to-center distance R for the molecular structure of **5**.

moments. The medium is considered by the square of the refractive index n multiplied with the vacuum permittivity ε_0. The transition dipole moment of a monomeric BODIPY unit is polarized along the β-positions, known from thin-film examinations and quantum-chemical calculations.[38,45] Therefore, the subchromophoric dipole vectors have been marked as lines between these positions into the molecular structure of the dimer. The centroids of the six-membered C_3BN_2 rings served as centers of point dipoles. Figure 16 (bottom) illustrates this procedure for DYEmer **5**. With κ and R (in Å) from the molecular structure (either from XRD or DFT studies) and with $\mu_{eg}^{monomer}$ (in Cm) from the integration of the main absorption band of the monomeric reference **8** or **11**, the exciton splitting energy V_{AB} (in J) of the dimer can be calculated. The intensity ratio of the two exciton splitted absorption bands $D_{eg\pm}^{dimer}$ is given by the ratio of the dipole strengths relative to the monomer, which is only depending on the angle θ_{AB} between the subchromophores given by Equation (3):

$$D_{eg\pm}^{dimer} = \left|\mu_{eg\pm}^{dimer}\right|^2 = D_{eg}^{monomer} \cdot (1 \pm \cos\theta_{AB}) \quad (3)$$

Table 3 and Figures 17–19 summarize the results from the calculations using Kasha's model.

Table 3. Angle relation and center-to-center distance between the subchromophores, orientation factor κ and ratio of the relative dipole strengths for the molecular structures from X-ray diffraction (**5**, **6**, **10**) and from quantum-chemical calculations for a CH_2Cl_2 solution (**5-I/II**, **6-I/II/III**, **10′-I/II/III**).

Cpd.[a,b]	θ_A [°]	θ_B [°]	θ_{AB} [°]	R [Å]	κ	$D_{eg+}^{dimer}/D_{eg-}^{dimer}$
5	26.61(2)	40.81(2)	49.67(3)	7.803(1)	−1.38	1.65:0.35
5-I	31.89	31.88	40.16	7.901	−1.40	1.76:0.24
5-II	59.63	59.63	71.48	6.041	−0.45	1.32:0.68
6	34.33(2)	41.89(2)	57.19(3)	8.541(1)	−1.30	1.54:0.46
6-I	40.86	41.73	62.69	8.710	−1.23	1.46:0.54
6-II	38.27	71.83	84.85	7.601	−0.64	1.09:0.91
6-III	57.33	57.34	68.32	6.455	−0.50	1.37:0.63
10	37.19(2)	37.19(2)	74.36(3)	8.193(1)	−1.63	1.27:0.73
	37.11(2)	37.11(2)	74.09(4)	8.199(1)	−1.63	1.27:0.73
10′-I	35.41	35.56	70.93	8.362	−1.66	1.33:0.67
10′-II	35.39	35.40	70.75	8.262	−1.66	1.33:0.67
10′-III	35.06	35.98	71.04	8.306	−1.66	1.32:0.68

[a] For **8**: $\mu = 3.43 \times 10^{-29}$ Cm (at $\lambda_{max} = 545$ nm in CH_2Cl_2). [b] For **11**: $\mu = 2.53 \times 10^{-29}$ Cm (at $\lambda_{max} = 524$ nm in CH_2Cl_2).

In the case of **5** the measured intensity ratio of the excitonic absorptions is approximated equally well by the solution minimum conformation **5-I** and by the conformation in the crystalline state. Due to the rather high energy level, the conformational state **5-II** appears to play only a negligible role. However, the observed absorption spectrum deviates markedly from the calculated data by the strength of the excitonic splitting, and by the center of gravity of the excitonic absorption. This former finding is presumably being caused by the oversimplifying description of the solvation by a homogeneous dielectric field and the approximation of the transition dipole moment as a point dipole, while the observed red shift of the absorption bands indicates significant conjugation between the two BODIPY subchromophores through a free 3p electron pair of the sulfur bridge. The same explanations can be used to also discuss the differences between the calculated and the measured spectra of **10**/**10′**. Other than above, however, only a slight bathochromic shift is observed in the measurement. This indicates a smaller degree of conjugation in **10** as expected for the special conformations of this DYEmer in the solid and in solution.

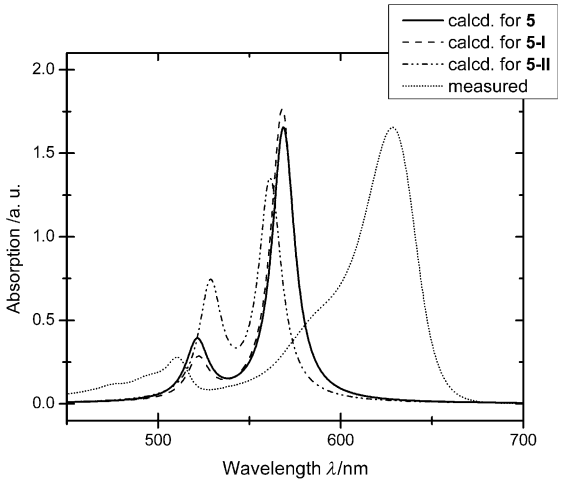

Figure 17. Comparison of measured and calculated absorption bands for the crystallographic conformer and for two calculated low-energy conformers of **5** (CH_2Cl_2). The calculated curves of the main absorption as a function of the wavelength are given by the sum of the two exciton bands assuming Lorentz band shape with a half width of 15 nm.

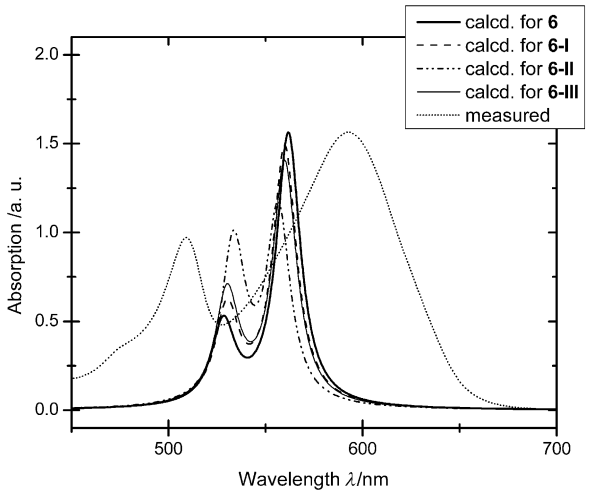

Figure 18. Comparison of measured and calculated absorption bands for the crystallographic conformer and for three calculated low-energy conformers of **6** (CH_2Cl_2). The calculated curves of the main absorption as a function of the wavelength are given by the sum of the two exciton bands assuming Lorentz band shape with a half width of 15 nm.

For the three lowest-energy conformers of the disulfide **6**, significantly different optical absorption spectra are proposed (Figure 18). The measured intensity ratio of the exci-

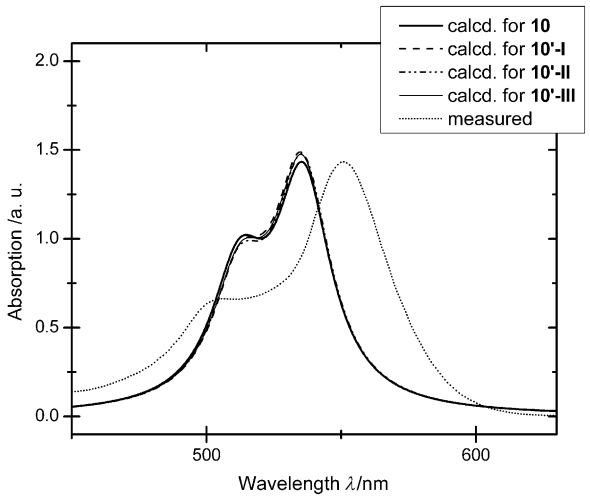

Figure 19. Comparison of measured and calculated absorption bands for the crystallographic conformer and for three calculated low-energy conformers of **10**/**10′** (CH_2Cl_2). The calculated curves of the main absorption as a function of the wavelength are given by the sum of the two exciton bands assuming Lorentz band shape with a half width of 25 nm.

tonic splitting is best reproduced by a weighted mixture of the three most favorable conformers **6-I**, **6-II**, and **6-III**, although again the strengths of the splitting is much smaller than in the real spectrum.

Electrochemical investigations: Cyclic voltammetry of the three S-bridged DYEmers **5**, **6**, and **10**, and the two reference compounds **8** and **11** was carried out in dry CH_2Cl_2 (0.5 mol L^{-1} $n$$Bu_4NPF_6$), using ferrocene as the internal standard. The obtained potentials are listed in Table 4. The

Table 4. Electrochemical potentials of the sulfur-containing BODIPYs in CH_2Cl_2 (0.5 mol L^{-1} $n$$Bu_4NPF_6$) versus ferrocene as internal standard at room temperature.

Compound	$E^{red}_{1/2}$ [V] (ΔE_p [mV])		$E^{ox}_{1/2}$ [V] (ΔE_p [mV])		E^{red}_p [V]	E^{ox}_p [V]
	A^-/A	A^{2-}/A^-	A^+/A	A^{2+}/A^+	$2RS^-/(RS)_2$	
5	−1.40	−1.77	0.48	0.88	–	–
	(irr.)	(90)	(80)	(150)		
6	−1.44	−1.79	0.55	0.91	−1.22	−0.33
	(irr.)	(70)	(210)	(150)		
8	−1.47	–	0.54	–	–	–
	(irr.)		(100)			
10	−1.55	−1.67	0.59	0.91	–	–
	(irr.)	(120)	(100)	(130)		
11	−1.55	–	0.68	–	–	–
	(irr.)		(160)			

cyclic voltammograms for the BODIPYs **8** and **11** (see Supporting Information) are similar and characteristic for monomeric BODIPYs. In either case the voltammogram displays one one-electron oxidation and one one-electron reduction. The oxidation step at 0.54 V (**8**) and 0.68 V (**11**) is electrochemically quasi-reversible ($i_{pa}/i_{pc} \approx 1$), while the reduction step at −1.47 V (**8**) and −1.55 V (**11**) is irreversible with an associated wave on the oxidation side ($E^{ox}_p = -0.53$ V for **8** and $E^{ox}_p = -0.60$ V for **11**). This irreversible reduction process is typical for *meso*-free BODIPYs.[46] There is no sign of electrochemical activity associated with the tolyl thioether moiety in either derivative. The major difference between the monomeric compounds is that the electrochemical bandgap of **11** is significantly larger (220 mV) than that of **8**. This compares well to the differences in the optical spectra of these BODIPYs.

The cyclic voltammogram of the sulfide **5** indicates the dimeric nature of the compound by electronic communication between the subunits (Figure 20). The above-mentioned oxidation and reduction processes for a single *meso*-free BODIPY unit are now split into two monoelectronic redox processes each, assuming an EE mechanism. The reversible oxidation to the radical monocation is slightly easier than for the monomer **8**. The quasi-reversible oxidation to the dication occurs at 0.88 V, which means that both oxidation steps are well separated with a split of ~400 mV. The first reduction step of **5** to the radical monoanion at −1.40 V shows the same irreversible feature as for **8**. The second reduction step to the dianion occurs clearly separated from the first step at −1.77 V and is quasi-reversible. Again, no sign of electrochemical activity can be associated with the sulfide bridge. The high degree of electronic interaction between the subunits of dimer **5**, which is apparent from the clear separation of the redox waves, reflects also the strong exciton coupling in the absorption spectrum. A similar correlation has been seen for other DYEmers before.[12,14,15,47]

Similar to **5**, a doubling of the number of waves for oxidation and reduction is observed in the cyclic voltammogram of the disulfide **6** (Figure 20). The potentials of the reduction steps to the monoanion and the dianion by consecutive electron transfers onto the BODIPY moieties are similar to those of the sulfide **5** and show a separation of ~350 mV. The first and second oxidation of **6** are also split with

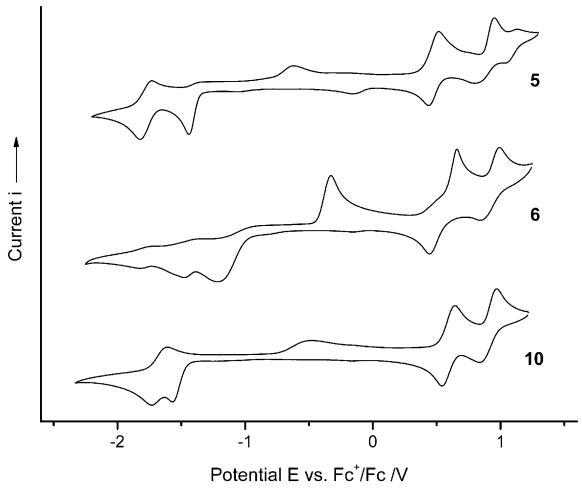

Figure 20. Cyclic voltammograms of **5** (5.8 mmol L^{-1}), **6** (4.4 mmol L^{-1}), and **10** (3.1 mmol L^{-1}) in CH_2Cl_2 containing $n$$Bu_4NPF_6$ (0.5 mol/L) at a scan rate of 50 mV s^{-1} (**5**) resp. 100 mV s^{-1} (**6**, **10**) at room temperature.

~360 mV, and the potential of the first oxidation is very similar to that for the monomeric **8**. In addition to these typical characteristics of such a DYEmer, **6** shows an additional redox process with a reduction at −1.22 V and a significantly displaced back oxidation at −0.33 V. Each process represents a two-electron transfer and can be assigned to a disulfide/twofold thiolate transition. Related diaryl disulfides $(RS)_2$ are electrochemically reduced by an ECE mechanism to two thiolate anions RS^- in an (electro)chemically reversible process.[48] The large peak separation of disulfide cleavage and formation of ~890 mV for **6** indicates significant kinetic hindrance and therefore bistability of the chemically reversible disulfide/thiolate couple over this potential range.

The sulfide **10** exhibits a similar cyclic voltammogram (Figure 20) as the sulfide **5** with a first irreversible and a second quasi-reversible reduction step, and with two quasi-reversible one-electron oxidation processes. The electronic communication between the subunits is obviously effective through the β-positions, too. Compared to the α-bridged dimer **5**, however, the splitting of the redox processes of 320 mV for the oxidation and 120 mV for the reduction side is smaller for **10**, and in particular the two consecutive reduction peaks are not as well separated. The smaller potential splitting corresponds with a less pronounced exciton coupling in the absorption spectrum of **10**. Similar differences between α,α- and β,β-coupled DYEmers have been found earlier for the directly C–C coupled derivatives.[14,15,47] Furthermore, the potential of the first oxidation of **10** is slightly more positive than those of the two other DYEmers **5** and **6**, and the first reduction wave occurs at a more negative potential of −1.55 V, which results in a larger electrochemical band gap for **10**.

Conclusion

In summary, we have shown that different sulfur-bridged DYEmers are available from simple BODIPY precursors by nucleophilic and electrophilic aromatic substitution reactions, and that the photophysical and electrochemical properties of these DYEmers are clearly distinct from those of the monomers due to intense communication between the BODIPY subunits. The structures of the DYEmers in the solid state and in solution have been analyzed in some detail and show far reaching similarities with respect to the lowest-energy conformers, despite the fact that packing effects are clearly present in the crystalline states.

If the conformations and relative orientations of the BODIPY subunits in a DYEmer chromophore are known, an application of the Kasha model provides well adapted information concerning the intensity ratio of the exciton splitting in all cases. The strength of the excitonic splitting, however, is generally underestimated by this method. We account an oversimplified description of the solvation and the point-dipole approximation used by the Kasha model for this deviation, although other aspects certainly also contribute to this effect. Additional bathochromic shifts are observed if an electronic conjugation between the BODIPY subunits is conformationally possible and effective through the sulfur bridge. With these deviations in mind, the Kasha model of excitonic coupling in combination with a conformational analysis provides a simple and acceptable method for a qualitative prediction of optical absorption characteristics for the class of BODIPY-based DYEmers.

Experimental Section

General: Solvents were dried according to standard procedures under inert gas atmosphere of argon or nitrogen. All reagents were purchased from commercial sources in reagent grade and used as received, unless stated otherwise. NMR spectra were obtained by using a Bruker DRX 400 and a Bruker Avance 300 spectrometer with room temperature as measuring temperature, if not otherwise indicated. Chemical shifts (δ) are given in ppm relative to residual protio solvent resonances (^{1}H, ^{13}C NMR spectra) or to external standards ($BF_3{\cdot}Et_2O$ for ^{11}B and $CFCl_3$ for ^{19}F NMR spectra). High-resolution ESI mass spectra were recorded with a Finnigan LTQ FT. MALDI-TOF spectra were recorded on a Bruker Biflex IV with sinapinic acid in MeCN as matrix. A Shimadzu UV-1601 PC spectrophotometer and a Varian Cary Eclipse spectrofluorometer were used to acquire absorption, emission, and excitation spectra. Absolute fluorescence quantum yields were determined in aerated solvents by a PTI QuantaMaster 40 UV VIS spectrofluorometer equipped with an integrating sphere. The provided corrections for excitation and emission were applied. Cyclic voltammetry was performed with a Princeton Applied Research VersaSTAT 3 potentiostat under inert conditions at room temperature in absolute CH_2Cl_2 containing nBu$_4$NPF$_6$. A self-made 3-electrode set-up with two platinum wires as working and counter electrodes and a silver wire as quasi-reference electrode was used and ferrocene as internal standard had been added. Single-crystal X-ray diffraction studies were performed by using a Stoe IPDS-I X-ray diffractometer (**8**) or an Oxford Diffraction Xcalibur diffractometer with an Atlas (Nova) detector (**5**, **6**, **10**, **11**). All structures were solved and refined by using the SHELXS programs for crystal structure determination[49] and refinement.[50] The gas phase global minima of **5**, **6**, and **10′** were obtained by first applying an extended conformational analysis using the OPLS_2005 force field[51] together with a Monte Carlo torsional sampling as implemented in the Macromodel (BatchMin 9.9) program.[52] The lowest-energy conformations of **5**, **6**, and **10′** have then been further optimized by applying density functional theory. For all optimizations and subsequent calculations the B3LYP hybrid density functional[53] as implemented in the Gaussian09 set of programs[54] was employed. All atoms were described by standard double zeta all electron basis set augmented with one set of polarization functions (6-31G(d,p)). First a geometry optimization was carried out out for a single molecule in an implicit solvent (dichloromethane). Solvent effects were incorporated by employing the polarizable continuum model (PCM).[55] After the relevant stationary points were localized on the energy surface, they were further characterized as minima states by normal mode analysis based on the analytical energy second derivatives. Enthalpic and entropic contributions were calculated by statistical thermodynamics as implemented in the Gaussian09 set of programs.[54]

Bis-(1,2,5,6,7-pentamethyl-4,4-difluoro-4-bora-3a,4a-diaza-*s*-indacen-3-yl)-sulfide (5): To a suspension of **4** (199 mg, 0.584 mmol) in toluene (11 mL) a solution of $Na_2S{\cdot}9H_2O$ (77 mg, 0.321 mmol) in H_2O (174 μL) and nBu$_4$NBr (catalytic amount) were added. The mixture was heated to reflux for 3.5 h with a color change to dark violet. After cooling the solvent was removed on a rotary evaporator. By column chromatography (silica, CH_2Cl_2) the product was separated in the fourth colorful, deep blue fraction. After evaporation of the solvent and drying in vacuo the product was obtained as dark violet plates with intense green shine (91 mg, 56%). ^{1}H NMR (400 MHz, CD_2Cl_2): δ = 7.04 (s, 2H, 8/8′-C*H*), 2.51 (s, 6H, 5/5′-CCH_3), 2.19 (s, 6H, 7/7′-CCH_3), 2.13 (s, 6H, 1/1′-CCH_3),

1.96 (s, 6H, 6/6′-CCH_3), 1.60 ppm (s, 6H, 2/2′-CCH_3); ^{13}C NMR (100 MHz, CD_2Cl_2): δ = 160.4 (2C, 5/5′-CCH_3), 142.2 (2C, 3/3′-C*S*), 139.9 (2C, 7/7′-CCH_3), 136.5 (2C, 1/1′-CCH_3), 134.9 (2C, 7a/7′a-C), 133.3 (2C, 8a/8′a-C), 130.2 (2C, 2/2′-CCH_3), 128.1 (2C, 6/6′-CCH_3), 118.8 (2C, 8/8′-C*H*), 13.5 (2C, 5/5′-CCH_3), 10.0 (4C, 1/1′-CCH_3, 7/7′-CCH_3), 9.3 (2C, 2/2′-CCH_3), 9.1 ppm (2C, 6/6′-CCH_3); ^{19}F NMR (376 MHz, CD_2Cl_2): δ = −138.8 (br s, 2F, 2×B*F*F), −147.7 ppm (br s, 2F, 2×BF*F*); ^{19}F NMR (282 MHz, [D$_6$]DMSO): δ = −136.7 (br s, 2F, 2×B*F*F), −146.1 ppm (br s, 2F, 2×BF*F*); ^{11}B NMR (128 MHz, CD_2Cl_2): δ = 0.54 ppm (pseudo t, J_{BF} = 33 Hz, 2B, 2×BF_2); MS (MALDI-TOF): *m*/*z*: 554 [*M*]$^+$; MS (ESI): *m*/*z*: 577 [*M*+Na]$^+$, 535 [*M*−F]$^+$; HRMS (ESI): *m*/*z*: calcd for $C_{28}H_{32}B_2F_4N_4SNa$ [*M*+Na]$^+$: 577.2362; found: 577.2362.

To a solution of **3** (32 mg, 0.122 mmol) in dry CH_2Cl_2 (13 mL) every hour SCl_2 (4×5 μL, 4×0.067 mmol) was added at 0 °C. After each addition the ice bath was removed and meanwhile the mixture was stirred at room temperature. The initially orange solution turned violet after complete addition. After 5 h the solvent was removed on a rotary evaporator and the residue was purified by column chromatography (silica, CH_2Cl_2). The deep blue fraction gave after evaporation and drying in vacuo product **5** (8 mg, 24 %).

Bis-(1,2,5,6,7-pentamethyl-4,4-difluoro-4-bora-3a,4a-diaza-*s*-indacen-3-yl)-disulfide (6): To an orange solution of **4** (50 mg, 0.147 mmol) in CH_2Cl_2 (12 mL) a freshly prepared yellow solution of Na_2S·9H_2O (20 mg, 0.083 mmol) and S (2.7 mg, 0.083 mmol) in MeOH (1 mL) was added and stirred at room temperature. After 25 min the reaction was quenched by filtering the now deep red reaction mixture through a short plug of silica with CH_2Cl_2/Et_2O 2:1. After evaporation the residue was purified by column chromatography (silica, CH_2Cl_2/Et_2O 49:1). First, residual starting material was eluted (2 mg, 4 %), then the product as a blue-violet fraction without visible fluorescence. After evaporation and drying in vacuo the product was obtained as a dark violet, microcrystalline solid with intense green shine (29 mg, 67 %). ^{1}H NMR (400 MHz, CD_2Cl_2): δ = 7.08 (s, 2H, 8/8′-C*H*), 2.54 (s, 6H, 5/5′-CCH_3), 2.20 (s, 6H, 7/7′-CCH_3), 2.14 (s, 6H, 1/1′-CCH_3), 1.97 (s, 6H, 6/6′-CCH_3), 1.79 ppm (s, 6H, 2/2′-CCH_3); ^{13}C NMR (100 MHz, CD_2Cl_2): δ = 164.3 (2C, 5/5′-CCH_3), 142.4 (2C, 3/3′-C*S*), 141.1 (2C, 7/7′-CCH_3), 136.7 (2C, 7a/7′a-C), 135.0 (2C, 8a/8′a-C), 133.9 (2C), 132.6 (2C), 129.5 (2C, 6/6′-CCH_3), 119.7 (2C, 8/8′-C*H*), 13.9 (2C, 5/5′-CCH_3), 10.1 (2C, 1/1′-CCH_3), 10.0 (2C, 7/7′-CCH_3), 9.8 (2C, 2/2′-CCH_3), 9.4 ppm (2C, 6/6′-CCH_3); ^{19}F NMR (376 MHz, CD_2Cl_2): δ = −141.9 ppm (q, J_{BF} = 31 Hz, 4F, 2×BF_2); ^{11}B NMR (128 MHz, CD_2Cl_2): δ = 0.89 ppm (t, J_{BF} = 31 Hz, 2B, 2×BF_2); MS (ESI): *m*/*z*: 609 [*M*+Na]$^+$; HRMS (ESI): *m*/*z*: calcd for $C_{28}H_{32}B_2F_4N_4S_2Na$ [*M*+Na]$^+$: 609.2083; found: 609.2083.

To a solution of **3** (84 mg, 0.320 mmol) in dry CH_2Cl_2 (6 mL) at −65 °C a solution of S_2Cl_2 (15 μL, 0.184 mmol) in dry CH_2Cl_2 (1 mL) was added dropwise within 25 min. After complete addition the reaction mixture was stirred until warmed up to room temperature. The organic phase was washed with H_2O (10 mL) and then the solvent was removed on rotary evaporator. The residue was separated by column chromatography (silica, CH_2Cl_2). First, a violet fraction was eluted (presumably the trisulfide (MS (ESI): *m*/*z*: 641 [*M*+Na]$^+$; HRMS (ESI): *m*/*z*: calcd for $C_{28}H_{32}B_2F_4N_4S_3Na$ [*M*+Na]$^+$: 641.1804; found: 641.1805; also tetrasulfide detected: MS (ESI): *m*/*z*: 673 [*M*+Na]$^+$; HRMS (ESI): *m*/*z* calcd for $C_{28}H_{32}B_2F_4N_4S_4Na$ [*M*+Na]$^+$: 673.1524; found: 673.1533), but instable with decomposition to sulfide **5** and disulfide **6**), then the blue fraction of the sulfide **5**, finally the blue-violet fraction of the disulfide **6**. Both isolable products were freed from the solvent in vacuo (**5**: 19 mg, 21 %; **6**: 31 mg, 33 %).

2,3,7,8,9-Pentamethyldipyrrin-1-thione (7): A suspension of **4** (42 mg, 0.123 mmol) in toluene (4 mL) was heated to 90 °C and a solution of Na_2S·9H_2O (21 mg, 0.088 mmol) and S (3 mg, 0.088 mmol) in EtOH/H_2O (5 mL, 4:1) was added. The reaction mixture was kept at 90 °C for 2 h. After cooling the solvent was reduced on a rotary evaporator and the dark red residue was purified by column chromatography (silica, CH_2Cl_2, then CH_2Cl_2/EtOAc 9:1). The red product fraction gave a red-black solid (24 mg, 78 %). ^{1}H NMR (300 MHz, $CDCl_3$): δ = 11.16 (br s, 1H, N*H*), 9.75 (br s, 1H, N*H*), 6.24 (s, 1H, C*H*), 2.37 (s, 3H, CH_3), 2.11 (s, 3H, CH_3), 2.09 (s, 3H, CH_3), 2.07 (s, 3H, CH_3), 1.91 ppm (s, 3H, CH_3); ^{13}C NMR (100 MHz, $CDCl_3$): δ = 186.2, 139.9, 136.1, 132.9, 130.1, 123.6, 118.7, 104.1, 12.1 (CH_3), 10.7 (CH_3), 10.5 (CH_3), 10.1 (CH_3), 9.0 ppm (CH_3); MS (ESI): *m*/*z*: 269 [*M*+Na]$^+$, 247 [*M*+H]$^+$; HRMS (ESI): *m*/*z*: calcd for $C_{14}H_{19}N_2S$ [*M*+H]$^+$: 247.1263; found: 247.1270.

1,2,5,6,7-Pentamethyl-3-(4-methylphenylthio)-4,4-difluoro-4-bora-3a,4a-diaza-*s*-indacene (8): To an orange-yellow solution of **4** (48 mg, 0.141 mmol) in a mixture of MeCN (40 mL) and CH_2Cl_2 (10 mL) NEt_3 (29 μL, 0.211 mmol) was added at room temperature. Then addition of 4-methylthiophenol (28 mg, 0.225 mmol) followed, whereupon the solution rapidly turned red-orange. After 15 min the reaction mixture was poured into CH_2Cl_2 (100 mL), washed with saturated aqueous NaCl solution (20 mL) and H_2O (20 mL), dried over Na_2SO_4, and the solvent was removed on a rotary evaporator. Purification by column chromatography (silica, CH_2Cl_2/*n*-pentane 1:1) gave the product as red-orange fraction of orange fluorescence, which was obtained after drying in vacuo as red, microcrystalline solid with golden shine (39 mg, 72 %). ^{1}H NMR (400 MHz, $CDCl_3$): δ = 7.20 (m, ^3J = 8.2 Hz, 2H, 2×*meta*-tolyl-C*H*), 7.04 (m, 2H, 2×*ortho*-tolyl-C*H*), 6.99 (s, 1H, 8-C*H*), 2.53 (s, 3H, 5-CCH_3), 2.28 (s, 3H, tolyl-CH_3), 2.16 (s, 3H, 7-CCH_3), 2.13 (s, 3H, 1-CCH_3), 1.94 (s, 3H, 6-CCH_3), 1.77 ppm (s, 3H, 2-CCH_3); ^{13}C NMR (75 MHz, $CDCl_3$): δ = 161.1 (1C, 5-CCH_3), 143.0 (1C, 3-C*S*), 139.7 (1C, 7-CCH_3), 136.3 (1C, tolyl-CCH_3), 135.5 (1C, 1-CCH_3), 134.9 (1C, 7a-C), 132.8 (1C, 8a-C), 132.2 (1C, tolyl-C*S*), 130.0 (1C, 2-CCH_3), 129.8 (2C, 2×*ortho*-tolyl-C*H*), 129.5 (2C, 2×*meta*-tolyl-C*H*), 127.7 (1C, 6-CCH_3), 118.8 (1C, 8-C*H*), 21.2 (1C, tolyl-CH_3), 13.3 (br s, 1C, 5-CCH_3), 9.9 (1C, 1-CCH_3), 9.9 (1C, 2-CCH_3), 9.8 (1C, 7-CCH_3), 9.1 ppm (1C, 6-CCH_3); ^{19}F NMR (188 MHz, $CDCl_3$): δ = −143.4 ppm (q, J_{BF} = 32 Hz, 2F, BF_2); ^{11}B NMR (96 MHz, $CDCl_3$): δ = 0.99 ppm (t, J_{BF} = 32 Hz, 1B, BF_2); MS (ESI): *m*/*z*: 407 [*M*+Na]$^+$; HRMS (ESI): *m*/*z*: calcd for $C_{21}H_{23}BF_2N_2SNa$ [*M*+Na]$^+$: 407.1535; found: 407.1539.

Bis-(6-ethyl-1,3,5,7-tetramethyl-4,4-difluoro-4-bora-3a,4a-diaza-*s*-indacen-2-yl)-sulfide (10): To an orange solution of **9** (60 mg, 0.219 mmol) in dry CH_2Cl_2 (6 mL) a solution of S_2Cl_2 (11 μL, 0.138 mmol) in dry CH_2Cl_2 (2 mL) was added at −70 °C slowly within 2 h. After complete addition the now red reaction mixture was quenched with H_2O (20 mL) and warmed up to room temperature. After phase separation the organic phase was dried over Na_2SO_4 and the solvent was removed on a rotary evaporator. The residue was purified by column chromatography (silica, CH_2Cl_2/*n*-pentane 1:1). First, some orange to red-orange fractions without visible fluorescence were eluted (presumably disulfides according to mass spectrometry), then the violet-red main fraction without visible fluorescence of the sulfide **10** was eluted. The isolable product was freed from the solvent in vacuo and gave a red, microcrystalline solid (16 mg, 25 %). ^{1}H NMR (400 MHz, $CDCl_3$): δ = 6.97 (s, 2H, 8/8′-C*H*), 2.57 (s, 6H, 3/3′-CCH_3), 2.51 (s, 6H, 5/5′-CCH_3), 2.39 (q, ^3J = 7.6 Hz, 4H, 6/6′-CCH_2), 2.18 (s, 6H, 1/1′-CCH_3), 2.17 (s, 6H, 7/7′-CCH_3), 1.06 ppm (t, ^3J = 7.6 Hz, 6H, 2×CH_2CH_3); ^{13}C NMR (100 MHz, $CDCl_3$): δ = 158.8 (2C, 5/5′-CCH_3), 155.8 (2C, 3/3′-CCH_3), 140.5 (2C, 1/1′-CCH_3), 138.8 (2C, 7/7′-CCH_3), 134.0 (2C, 7a/7′a-C), 133.5 (2C, 6/6′-CCH_2), 131.4 (2C, 8a/8′a-C), 119.4 (4C, 8/8′-C*H* and 2/2′-C*S*), 17.4 (2C, 6/6′-CCH_2), 14.5 (2C, 2×CH_2CH_3), 13.2 (br s, 2C, 3/3′-CCH_3), 13.0 (br s, 2C, 5/5′-CCH_3), 10.7 (2C, 1/1′-CCH_3), 9.6 ppm (2C, 7/7′-CCH_3); ^{19}F NMR (376 MHz, $CDCl_3$): δ = −146.7 ppm (q, J_{BF} = 33 Hz, 4F, 2×BF_2); ^{11}B NMR (128 MHz, $CDCl_3$): δ = 0.78 ppm (t, J_{BF} = 33 Hz, 2B, 2×BF_2); MS (ESI): *m*/*z*: 605 [*M*+Na]$^+$, 582 [*M*]$^+$, 563 [*M*−F]$^+$; HRMS (ESI): *m*/*z*: calcd for $C_{30}H_{36}B_2F_4N_4S$ [*M*]$^+$: 582.2777; found: 582.2787.

6-Ethyl-1,3,5,7-tetramethyl-2-(4-methylphenylthio)-4,4-difluoro-4-bora-3a,4a-diaza-*s*-indacene (11): To an orange-yellow solution of **9** (107 mg, 0.387 mmol) in dry CH_2Cl_2 (26 mL) at 0 °C a solution of 4-methylphenylsulfenyl chloride (167 mmol L^{-1} in CH_2Cl_2) (2.8 mL, 0.470 mmol) was added dropwise within 15 min. After complete addition H_2O (20 mL) was added to the deep red reaction mixture. After phase separation the organic phase was washed with H_2O (20 mL), dried over Na_2SO_4, and the solvent was removed on a rotary evaporator. Purification by column chromatography (silica, CH_2Cl_2/*n*-pentane 1:1) gave the product as red fraction of orange fluorescence, which was obtained after drying in vacuo as red, microcrystalline solid (146 mg, 96 %). ^{1}H NMR (400 MHz, $CDCl_3$): δ = 7.08 (s, 1H; 8-C*H*), 7.03 (m, ^3J = 8.2 Hz, 2H; 2×tolyl-*meta*-

C*H*), 6.95 (m, ^3J = 8.2 Hz, 2H; 2×tolyl-*ortho*-C*H*), 2.55 (s, 6H; 3/5-CCH_3), 2.42 (q, ^3J = 7.6 Hz, 2H; 6-CCH_2), 2.28 (s, 3H; tolyl-CH_3), 2.24 (s, 3H; 1-CCH_3), 2.20 (s, 3H; 7-CCH_3), 1.09 ppm (t, ^3J = 7.6 Hz, 3H; CH_2CH_3); ^{13}C NMR (100 MHz, $CDCl_3$): δ = 159.6 (1C; 5-*C*CH_3), 157.3 (1C; 3-*C*CH_3), 143.1 (1C; 1-*C*CH_3), 139.3 (1C; 7-*C*CH_3), 134.9 (1C; tolyl-*C*CH_3), 134.5 (1C; tolyl-*C*S), 134.2 (1C; 8a-*C*), 133.8 (1C; 6-*C*CH_2), 131.4 (1C; 7a-*C*), 129.8 (2C; 2×tolyl-*meta*-C*H*), 126.1 (2C; 2×tolyl-*ortho*-C*H*), 119.8 (1C; 2-*C*S), 117.0 (1C; 8-*C*H), 21.0 (1C; tolyl-CH_3), 17.4 (1C; 6-CCH_2), 14.5 (1C; CH_2CH_3), 13.1 (br s, 1C; 3/5-CCH_3), 12.9 (br s, 1C; 3/5-CCH_3), 10.6 (1C; 1-CCH_3), 9.6 ppm (1C; 7-CCH_3); ^{19}F NMR (376 MHz, $CDCl_3$): δ = −146.6 ppm (q, J_{BF} = 33 Hz, 2F; BF_2); ^{11}B NMR (128 MHz, $CDCl_3$): δ = 1.04 ppm (t, J_{BF} = 33 Hz, 1B; *B*F_2); MS (ESI): *m*/*z*: 421 $[M+Na]^+$, 398 $[M]^+$, 383 $[M-CH_3]^+$; HRMS (ESI): *m*/*z*: calcd for $C_{22}H_{25}BF_2N_2SNa$ $[M+Na]^+$: 421.1692; found: 421.1695.

The solution of 4-methylphenylsulfenyl chloride was prepared by dropwise addition of a solution of 4-methylthiophenol (248 mg, 2 mmol) in dry CH_2Cl_2 (6 mL) to a suspension of *N*-chlorosuccinimide (267 mg, 2 mmol) in CH_2Cl_2 (6 mL) at room temperature. After stirring for 30 min the orange-yellow solution of the sulfenyl chloride was used in situ assuming a complete conversion (167 mmol L^{-1}).

Crystal data for 5: $C_{28}H_{32}B_2F_4N_4S$, M = 554.26, triclinic, space group $P\bar{1}$, a = 8.632(1), b = 11.111(1), c = 15.069(2) Å, α = 107.78(1), β = 96.81(1), γ = 99.02(1)°, V = 1337.6(3) Å^3, Z = 2, ρ_{calcd} = 1.376 g cm^{-3}, $\mu(Cu_{K\alpha})$ = 1.536 mm^{-1}, R_1 [$I > 2\sigma(I)$] = 0.0374, wR_2 (all data) = 0.1026.

Crystal data for 6: $C_{28}H_{32}B_2F_4N_4S_2$, M = 586.32, triclinic, space group $P\bar{1}$, a = 8.2876(8), b = 10.186(1), c = 18.139(2) Å, α = 83.293(8), β = 82.031(8), γ = 76.182(8)°, V = 1467.1(3) Å^3, Z = 2, ρ_{calcd} = 1.327 g cm^{-3}, $\mu(Cu_{K\alpha})$ = 2.078 mm^{-1}, R_1 [$I > 2\sigma(I)$] = 0.0421, wR_2 (all data) = 0.1083.

Crystal data for 8: $C_{21}H_{23}BF_2N_2S$, M = 384.28, monoclinic, space group $P2_1/c$, a = 8.124(1), b = 22.745(3), c = 10.977(1) Å, β = 107.00(2)°, V = 1939.7(4) Å^3, Z = 4, ρ_{calcd} = 1.316 g cm^{-3}, $\mu(Mo_{K\alpha})$ = 0.193 mm^{-1}, R_1 [$I > 2\sigma(I)$] = 0.0505, wR_2 (all data) = 0.1207.

Crystal data for 10: $C_{30}H_{36}B_2F_4N_4S$, M = 582.31, orthorhombic, space group *Pnc*2, a = 35.229(3), b = 8.7558(6), c = 9.2389(8) Å, V = 2849.8(4) Å^3, Z = 4, ρ_{calcd} = 1.357 g cm^{-3}, $\mu(Cu_{K\alpha})$ = 1.468 mm^{-1}, R_1 [$I > 2\sigma(I)$] = 0.0434, wR_2 (all data) = 0.1124.

Crystal data for 11: $C_{22}H_{25}BF_2N_2S$, M = 398.31, orthorhombic, space group *Pbca*, a = 17.5637(5), b = 9.8783(3), c = 23.4254(8) Å, V = 4064.3(2) Å^3, Z = 8, ρ_{calcd} = 1.302 g cm^{-3}, $\mu(Mo_{K\alpha})$ = 0.187 mm^{-1}, R_1 [$I > 2\sigma(I)$] = 0.0408, wR_2 (all data) = 0.1092.

Crystallographic data: CCDC-926196 (**5**), -926197 (**6**)-926198 (**8**)-926199 (**10**) and -926200 (**11**) contain the supplementary crystallographic data for this paper. These data can be obtained free of charge from The Cambridge Crystallographic Data Centre via www.ccdc.cam.ac.uk/data_request/cif.

Acknowledgements

Support for this work by the Deutsche Forschungsgemeinschaft (DFG) is gratefully acknowledged.

[1] A. Treibs, F.-H. Kreuzer, *Liebigs Ann. Chem.* **1968**, *718*, 208–223.
[2] G. Ulrich, R. Ziessel, A. Harriman, *Angew. Chem.* **2008**, *120*, 1202–1219; *Angew. Chem. Int. Ed.* **2008**, *47*, 1184–1201.
[3] A. Loudet, K. Burgess, *Chem. Rev.* **2007**, *107*, 4891–4932.
[4] a) M. P. Shandura, V. P. Yakubovskyi, A. O. Gerasov, O. D. Kachkovsky, Y. M. Poronik, Y. P. Kovtun, *Eur. J. Org. Chem.* **2012**, 1825–1834; b) T. Uppal, X. Hu, F. R. Fronczek, S. Maschek, P. Bobadova-Parvanova, M. G. H. Vicente, *Chem. Eur. J.* **2012**, *18*, 3893–3905.
[5] a) Y. Chen, J. Zhao, H. Guo, L. Xie, *J. Org. Chem.* **2012**, *77*, 2192–2206; b) T. Keyes, C. Long, R. Forster, A. Martin, *Chem. Commun.* **2012**, *48*, 5617–5619.
[6] a) L. Li, J. Han, B. Nguyen, K. Burgess, *J. Org. Chem.* **2008**, *73*, 1963–1970; b) S. L. Niu, G. Ulrich, R. Ziessel, A. Kiss, P.-Y. Renard, A. Romieu, *Org. Lett.* **2009**, *11*, 2049–2052; c) T. Bura, R. Ziessel, *Org. Lett.* **2011**, *13*, 3072–3075; d) S. Zhu, J. Zhang, G. Vegesna, F.-T. Luo, S. A. Green, H. Liu, *Org. Lett.* **2011**, *13*, 438–441.
[7] a) O. García, L. Garrido, R. Sastre, A. Costela, I. García-Moreno, *Adv. Funct. Mater.* **2008**, *18*, 2017–2025; b) J. Bañuelos, V. Martín, C. F. A. Gómes-Durán, I. J. A. Córdoba, E. Peña-Cabrera, I. García-Moreno, A. Costela, M. E. Pérez-Ojeda, T. Arbeloa, I. L. Arbeloa, *Chem. Eur. J.* **2011**, *17*, 7261–7270.
[8] M. Benstead, G. H. Mehl, R. W. Boyle, *Tetrahedron* **2011**, *67*, 3573–3601.
[9] a) G. Nöll, J. Daub, M. Lutz, K. Rurack, *J. Org. Chem.* **2011**, *76*, 4859–4873; b) C. Thivierge, A. Loudet, K. Burgess, *Macromolecules* **2011**, *44*, 4012–4015; c) S. Zhu, N. Dorh, J. Zhang, G. Vegesna, H. Li, F.-T. Luo, A. Tiwari, H. Liu, *J. Mater. Chem.* **2012**, *22*, 2781–2790.
[10] a) N. Saki, T. Dinc, E. U. Akkaya, *Tetrahedron* **2006**, *62*, 2721–2725; b) Y. Cakmak, S. Kolemen, S. Duman, Y. Dede, Y. Dolen, B. Kilic, Z. Kostereli, L. T. Yildirim, A. L. Dogan, D. Guc, E. U. Akkaya, *Angew. Chem.* **2011**, *123*, 12143–12147; *Angew. Chem. Int. Ed.* **2011**, *50*, 11937–11941; c) W. Wu, H. Guo, W. Wu, S. Ji, J. Zhao, *J. Org. Chem.* **2011**, *76*, 7056–7064; d) M. T. Whited, N. M. Patel, S. T. Roberts, K. Allen, P. I. Djurovich, S. E. Bradforth, M. E. Thompson, *Chem. Commun.* **2012**, *48*, 284–286; e) W. Pang, X.-F. Zhang, J. Zhou, C. Yu, E. Hao, L. Jiao, *Chem. Commun.* **2012**, *48*, 5437–5439; f) A. Poirel, A. De Nicola, P. Retailleau, R. Ziessel, *J. Org. Chem.* **2012**, *77*, 7512–7525.
[11] M. Bröring, R. Krüger, S. Link, C. Kleeberg, S. Köhler, X. Xie, B. Ventura, L. Flamigni, *Chem. Eur. J.* **2008**, *14*, 2976–2983.
[12] A. C. Benniston, G. Copley, A. Harriman, D. Howgego, R. W. Harrington, W. Clegg, *J. Org. Chem.* **2010**, *75*, 2018–2027.
[13] a) Y. Cakmak, E. U. Akkaya, *Org. Lett.* **2008**, *10*, 85–88; b) Y. Hayashi, S. Yamaguchi, W. Y. Cha, D. Kim, H. Shinokubo, *Org. Lett.* **2011**, *13*, 2992–2995; c) N. Sakamoto, C. Ikeda, M. Yamamura, T. Nabeshima, *Chem. Commun.* **2012**, *48*, 4818–4820; d) L. Gai, H. Lu, B. Zou, G. Lai, Z. Shen, Z. Li, *RSC Adv.* **2012**, *2*, 8840–8846; e) M. Nakamura, H. Tahara, K. Takahashi, T. Nagata, H. Uoyama, D. Kuzuhara, S. Mori, T. Okujima, H. Yamada, H. Uno, *Org. Biomol. Chem.* **2012**, *10*, 6840–6849.
[14] a) A. B. Nepomnyashchii, M. Bröring, J. Ahrens, A. J. Bard, *J. Am. Chem. Soc.* **2011**, *133*, 8633–8645; b) S. Rihn, M. Erdem, A. De Nicola, P. Retailleau, R. Ziessel, *Org. Lett.* **2011**, *13*, 1916–1919.
[15] A. B. Nepomnyashchii, M. Bröring, J. Ahrens, A. J. Bard, *J. Am. Chem. Soc.* **2011**, *133*, 19498–19504.
[16] M. Kasha, H. R. Rawls, M. Ashraf El-Bayoumi, *Pure Appl. Chem.* **1965**, *11*, 371–392.
[17] M. Baruah, W. Qin, R. A. L. Vallée, D. Beljonne, T. Rohand, W. Dehaen, N. Boens, *Org. Lett.* **2005**, *7*, 4377–4380.
[18] T. Rohand, M. Baruah, W. Qin, N. Boens, W. Dehaen, *Chem. Commun.* **2006**, 266–268.
[19] a) H. Falk, H. Flödl, *Monatsh. Chem.* **1989**, *120*, 45–51; b) A. K. Tipton, D. A. Lightner, A. F. McDonagh, *J. Org. Chem.* **2001**, *66*, 1832–1838.
[20] D. Sanchez-Garcia, T. Köhler, D. Seidel, V. Lynch, J. L. Sessler, *Chem. Commun.* **2005**, 2122–2124.
[21] S. M. Crawford, A. Thompson, *Org. Lett.* **2010**, *12*, 1424–1427.
[22] A. S. Semeikin, M. B. Berez, O. M. Chernova, E. V. Antina, S. A. Syrbu, T. V. Lyubimova, A. M. Kutepov, *Russ. Chem. Bull.* **2003**, *52*, 1807–1813.
[23] J. B. Paine, III, J. Hiom, D. Dolphin, *J. Org. Chem.* **1988**, *53*, 2796–2802.
[24] a) M. Liras, J. Bañuelos Prieto, M. Pintado-Sierra, F. López Arbeloa, I. García-Moreno, Á. Costela, L. Infantes, R. Sastre, F. Amat-Guerri, *Org. Lett.* **2007**, *9*, 4183–4186; b) J. Bañuelos, F. López Arbeloa, T. Arbeloa, S. Salleres, J. Vilas, F. Amat-Guerri, M. Liras, I. López Arbeloa, *J. Fluoresc.* **2008**, *18*, 899–907.
[25] S. Datta, D. A. Lightner, *Tetrahedron* **2009**, *65*, 77–82.
[26] L. Jiao, W. Pang, J. Zhou, Y. Wei, X. Mu, G. Bai, E. Hao, *J. Org. Chem.* **2011**, *76*, 9988–9996.

[27] V. Leen, T. Leemans, N. Boens, W. Dehaen, *Eur. J. Org. Chem.* **2011**, 4386–4396.
[28] a) X. Li, S. Huang, Y. Hu, *Org. Biomol. Chem.* **2012**, *10*, 2369–2372; b) V. Leen, P. Yuan, L. Wang, N. Boens, W. Dehaen, *Org. Lett.* **2012**, *14*, 6150–6153.
[29] D. A. Smithen, A. E. G. Baker, M. Offman, S. M. Crawford, T. S. Cameron, A. Thompson, *J. Org. Chem.* **2012**, *77*, 3439–3453.
[30] a) H. Seliger, H.-H. Görtz, *Synth. Commun.* **1980**, *10*, 175–182; b) K. M. Schlosser, A. P. Krasutsky, H. W. Hamilton, J. E. Reed, K. Sexton, *Org. Lett.* **2004**, *6*, 819–821.
[31] a) A. L. Spek, *PLATON, A Multipurpose Crystallographic Tool*, Utrecht University, Utrecht, The Netherlands, **2005**; b) P. van der Sluis, A. L. Spek, *Acta Crystallogr. Sect. A* **1990**, *46*, 194–201.
[32] A. K. Tipton, D. A. Lightner, *Monatsh. Chem.* **2002**, *133*, 707–716.
[33] **10′** is **10** with the 6,6′-ethyl substituents substituted for methyl.
[34] X. Xie, Y. Yuan, R. Krüger, M. Bröring, *Magn. Reson. Chem.* **2009**, *47*, 1024–1030; M. Bröring, Y. Yuan, R. Krüger, C. Kleeberg, X. Xie, *Z. Anorg. Allg. Chem.* **2010**, *636*, 518–523.
[35] E. Fron, E. Coutiño-Gonzalez, L. Pandey, M. Sliwa, M. Van der Auweraer, F. C. De Schryver, J. Thomas, Z. Dong, V. Leen, M. Smet, W. Dehaen, T. Vosch, *New J. Chem.* **2009**, *33*, 1490–1496.
[36] V. Leen, E. Braeken, K. Luckermans, C. Jackers, M. Van der Auweraer, N. Boens, W. Dehaen, *Chem. Commun.* **2009**, 4515–4517.
[37] a) K. Suzuki, A. Kobayashi, S. Kaneko, K. Takehira, T. Yoshihara, H. Ishida, Y. Shiina, S. Oishi, S. Tobita, *Phys. Chem. Chem. Phys.* **2009**, *11*, 9850–9860; b) C. Würth, C. Lochmann, M. Spieles, J. Pauli, K. Hoffmann, T. Schüttrigkeit, T. Franzl, U. Resch-Genger, *Appl. Spectrosc.* **2010**, *64*, 733–741.
[38] a) J. Karolin, L. B.-Å. Johansson, L. Strandberg, T. Ny, *J. Am. Chem. Soc.* **1994**, *116*, 7801–7806; b) F. Bergström, I. Mikhalyov, P. Hägglöf, R. Wortmann, T. Ny, L. B.-Å. Johansson, *J. Am. Chem. Soc.* **2002**, *124*, 196–204.
[39] a) W. Qin, T. Rohand, M. Baruah, A. Stefan, M. Van der Auweraer, W. Dehaen, N. Boens, *Chem. Phys. Lett.* **2006**, *420*, 562–568; b) W. Qin, V. Leen, T. Rohand, W. Dehaen, P. Dedecker, M. Van der Auweraer, K. Robeyns, L. Van Meervelt, D. Beljonne, B. Van Averbeke, J. N. Clifford, K. Driesen, K. Binnemans, N. Boens, *J. Phys. Chem. A* **2009**, *113*, 439–447.
[40] B. Ventura, G. Marconi, M. Bröring, R. Krüger, L. Flamigni, *New J. Chem.* **2009**, *33*, 428–438.
[41] T. Förster, *Pure Appl. Chem.* **1962**, *4*, 121–134.
[42] W. W. Parson, *Modern Optical Spectroscopy*, Springer, Berlin, **2009**, 281–295.
[43] B. Valeur, M. N. Berberan-Santos, *Molecular Fluorescence*, Wiley-VCH, Weinheim, **2012**.
[44] A. S. Davydov, *Theory of molecular excitons*, Plenum Press, New York, **1971**.
[45] J. Bañuelos Prieto, F. López Arbeloa, V. Martı'nez Martı'nez, I. López Arbeloa, *Chem. Phys.* **2004**, *296*, 13–22.
[46] a) M. Kollmannsberger, T. Gareis, S. Heinl, J. Breu, J. Daub, *Angew. Chem.* **1997**, *109*, 1391–1393; *Angew. Chem. Int. Ed. Engl.* **1997**, *36*, 1333–1335; b) R. Y. Lai, A. J. Bard, *J. Phys. Chem. B* **2003**, *107*, 5036–5042; c) A. B. Nepomnyashchii, S. Cho, P. J. Rossky, A. J. Bard, *J. Am. Chem. Soc.* **2010**, *132*, 17550–17559.
[47] A. B. Nepomnyashchii, M. Bröring, J. Ahrens, R. Krüger, A. J. Bard, *J. Phys. Chem. C* **2010**, *114*, 14453–14460.
[48] a) L. Meilin, J. V. Steven, C. D. J. Lutgard, *J. Electrochem. Soc.* **1989**, *136*, 2570–2575; b) S. Antonello, K. Daasbjerg, H. Jensen, F. Taddei, F. Maran, *J. Am. Chem. Soc.* **2003**, *125*, 14905–14916; c) H. Röhr, C. Trieflinger, K. Rurack, J. Daub, *Chem. Eur. J.* **2006**, *12*, 689–700.
[49] G. M. Sheldrick, *SHELXS-97*, *Program for the Solution of Crystal Structures*, University of Göttingen, Göttingen (Germany), **1997**.
[50] G. M. Sheldrick, *SHELXL-97*, *Program for the Refinement of Crystal Structures*, University of Göttingen, Göttingen (Germany), **1997**.
[51] W. L. Jorgensen, J. Tirado-Rives, *J. Am. Chem. Soc.* **1988**, *110*, 1657–1666.
[52] Macromodel, version 9.9, Schrödinger, LLC, New York, NY, **2012**.
[53] a) A. D. Becke, *Phys. Rev. B* **1988**, *38*, 3098–3100; b) C. Lee, W. Yang, R. G. Parr, *Phys. Rev. B* **1988**, *37*, 785–789.
[54] Gaussian 09, Revision A.02, M. J. Frisch, G. W. Trucks, H. B. Schlegel, G. E. Scuseria, M. A. Robb, J. R. Cheeseman, G. Scalmani, V. Barone, B. Mennucci, G. A. Petersson, H. Nakatsuji, M. Caricato, X. Li, H. P. Hratchian, A. F. Izmaylov, J. Bloino, G. Zheng, J. L. Sonnenberg, M. Hada, M. Ehara, K. Toyota, R. Fukuda, J. Hasegawa, M. Ishida, T. Nakajima, Y. Honda, O. Kitao, H. Nakai, T. Vreven, J. A. Montgomery, Jr., J. E. Peralta, F. Ogliaro, M. Bearpark, J. J. Heyd, E. Brothers, K. N. Kudin, V. N. Staroverov, R. Kobayashi, J. Normand, K. Raghavachari, A. Rendell, J. C. Burant, S. S. Iyengar, J. Tomasi, M. Cossi, N. Rega, J. M. Millam, M. Klene, J. E. Knox, J. B. Cross, V. Bakken, C. Adamo, J. Jaramillo, R. Gomperts, R. E. Stratmann, O. Yazyev, A. J. Austin, R. Cammi, C. Pomelli, J. W. Ochterski, R. L. Martin, K. Morokuma, V. G. Zakrzewski, G. A. Voth, P. Salvador, J. J. Dannenberg, S. Dapprich, A. D. Daniels, O. Farkas, J. B. Foresman, J. V. Ortiz, J. Cioslowski, D. J. Fox, Gaussian, Inc., Wallingford CT, **2009**.
[55] S. Miertuš, E. Scrocco, J. Tomasi, *Chem. Phys.* **1981**, *55*, 117–129.

Received: March 8, 2013
Revised: May 1, 2013
Published online: ■■ ■■, 0000

